

Numerical Study of Evaporative Cooling System Performance Using Well Water Driven by PV Panels on Thermal Comfort for Relief Tents

May Abdulazeez Rashid  *, Issam M.Ali Aljubury  

Department of Mechanical Engineering, College of Engineering, University of Baghdad, Baghdad, Iraq

ABSTRACT

When multitudes of people need to be evacuated from their homes for various reasons, including natural catastrophes and armed conflicts, time and money are of the essence. Therefore, emergency relief tents are considered the most effective option for this situation. However, the indoor environment of these tent types might be thermally uncomfortable, particularly on hot or extremely cold days. Different techniques were used to overcome this problem including evaporative cooling systems. The present study aims to use a numerical approach to assess the impact of utilizing a two-stage indirect/direct evaporative cooling system on enhancing the interior thermal comfort conditions of the relief tent. The numerical part was done by utilizing software that was written in Fortran language to simulate the case under various parameters, including changing the cellulose pad thickness and the volumetric water flow rates in the second heat exchanger of the indirect cooling stage. The selection of boundary conditions that were applied in numerical analysis was based on experimental data collected over specified days during the summer of 2022, in particular from July 15th to September 15th. According to the findings, having two heat exchangers in the indirect cooling stage of the cooling system helps keep the tent model at a comfortable temperature because of the exceptional performance of the proposed cooling system in lowering both dry and wet bulb air temperatures before entering the direct evaporative cooling stage. In addition, it was found that the indoor temperature drop increased by about 19% when increasing the thickness of the cellulose pad and raising the water flow rate in the second heat exchanger of the indirect cooling stage.

Keywords: Standardized emergency relief tent, Thermal comfort, Two-stage evaporative cooling system, PMV.


1. INTRODUCTION

Global epidemics, man-made conflicts, and other temporary difficulties that confront humanity force many people to escape in large numbers and compel them to reside in sheltering camps. As there are no alternative options for housing displaced persons

*Corresponding author

Peer review under the responsibility of University of Baghdad.

<https://doi.org/10.31026/j.eng.2024.08.12>

 This is an open access article under the CC BY 4 license (<http://creativecommons.org/licenses/by/4.0/>).

Article received: 09/09/2023

Article revised: 19/10/2023

Article accepted: 22/10/2023

Article published: 01/08/2024



immediately following a disaster (**Susanti, 2015**). The number of refugees who live in refugee camps exceeded eight million at the end of 2014 (**UNHCR, 2014**), and this number increased to more than nineteen million due to natural disasters in 2015 (**IDMC, 2017**), and in 2021, 82.4 million humans from the worldwide were forcefully displaced, with 20.7 million of them being refugees (**Tan and Tan, 2021; UN Refugee Agency, 2021**). The World Bank anticipated that owing to global warming as well as climate change, the number of migrants from the world's continents might exceed 216 million by (**World Bank Group, 2021; Xatamovich and Maidanovich, 2022**). The most prevalent approach for sheltering refugee people in these situations is to use emergency relief tents (**Poschl, 2017**). Shelter or Relief tent is considered a basic right for refugees and an essential component of humanitarian aid that plays an important role in the physical, mental and psychological health of people who are affected by disasters (**UNHCR, 1999**). However, these shelters were developed as temporary accommodations and cannot withstand strong climatic fluctuations. According to several studies, the temperature conditions in such shelters are substantially below typical comfort levels (**Albadra et al., 2017**). Thermal comfort can be defined as a state of satisfaction with the thermal conditions of the environment, or It is a lack of negative feelings caused by the thermal effects of the environment (**Fanger, 1981; Matusiak, 2010**). The preservation of the thermal balance between generating and loss of heat from the human body is necessary for ensuring thermal comfort (**Rupp et al., 2015**). Therefore, it is vital to evaluate thermal performance when researching sheltering alternatives for refugees. Thermal comfort in tents is affected by a variety of factors, including tent fabric type and its weight, resistance of water vapour permeability, tent framework brittleness, and resistance of tent fabric to tearing as well as water penetration (**IFRC, 2012**).

Therefore, several researchers studied the influence of the aforementioned parameters and focused their efforts on finding technical solutions to improve the thermal comfort inside the tents. For example: (**Crawford et al., 2005**) investigated the impact of fabric type on the tent's thermal comfort. They tested different types of fabrics and insulations in two identical models of tents under the frozen conditions of (-20°C) by carrying out the experiments in the warehouse freezer. The roof of the first model was covered by a composite layer of thermal insulation comprised of two polyethene sheets and a fibreglass layer in the middle, while in the second model, the roof and doors were covered by a composite layer consisting of stuffing bonded from the outer side to a hydrophilic membrane and separate breathable cover. The experiments' outcomes revealed that applying the suggested insulations in both tent models resulted in a significant fluctuation in temperature gradient with tent height. (**Zhang et al., 2017**) experimentally studied the influence of utilizing Retro-Reflective materials on lowering the impact of fallen solar radiation on a tent's roof and improving the interior thermal environment of the tent. The experiments were carried out in Chengdu, China, during the summer months. The results of the study revealed a rapid increase in both interior air temperature and inner surface radiation, especially when solar radiation is high, and it was demonstrated that using Retro-Reflective materials can lower the inner surface radiant temperature by up to (4.8) °C throughout the day. Furthermore, because of the powerful reflectivity of these materials to the sun's rays and their capacity to limit radiation heat gain throughout the summertime, the researchers proposed the Retro-Reflective materials as a promising choice for enhancing the interior thermal comfort of the tents. (**Gooijer et al. 2019**) conducted a theoretical analysis to investigate the impact of fabric type on the interior thermal comfort of tents. The researchers put seven different fabric types to the test, and they discovered that the type of tent fabric significantly influences the

permeability of water vapour, but it has no influence on the heat transfer process that is done between the interior and exterior of the tent.

In general, even with modifications, tents are unable to provide a good internal thermal environment and thus must be supplied with extra HVAC systems (Zemitis et al., 2021). One of the common simple systems that are used to improve the humidity level and hence, the interior thermal comfort of buildings in multiple applications including residential, agricultural, and industrial, is the evaporative cooling system. In comparison to mechanical vapor compression systems, evaporative cooling systems have several advantages. Including, using less electricity, enabling surplus electrical energy to be invested in other applications. Moreover, evaporative cooling systems use water as an operating fluid, so they reduce the volume of fossil fuels burned, which in turn minimizes the amount of released air pollutants-related environmental damage. Additionally, Evaporative Cooling system fabrication techniques are inexpensive and could be simply used in every country around the world (El-Dessouky, 2004). Evaporative cooling systems, as shown in Fig. 1, are classified into three types, which differ in terms of the technology used to reduce the temperature of the airflow. The first type is the direct evaporative cooling (DEC) system, which is based on removing the sensible heat of the hot outdoor air by evaporating water when passing airflow through wet cellulose pads, hence, the air leaves the system at a low temperature. However, this type of cooling system consumes large quantities of water that are difficult to provide particularly in desert regions. The second type is the Indirect evaporative cooling system which has the ability to solve air-conditioning issues related to energy usage and humidity level in the air. This system mainly consists of two channels: the dry main channel and the moist secondary channel. The sensible heat of exterior hot air is removed within the main channel at constant moisture content. Meanwhile, the surface temperature of the secondary channel drops because of the evaporation of the water layer that is located on the channel's surface due to spraying water on the secondary channel (Mohamed et al., 2020).

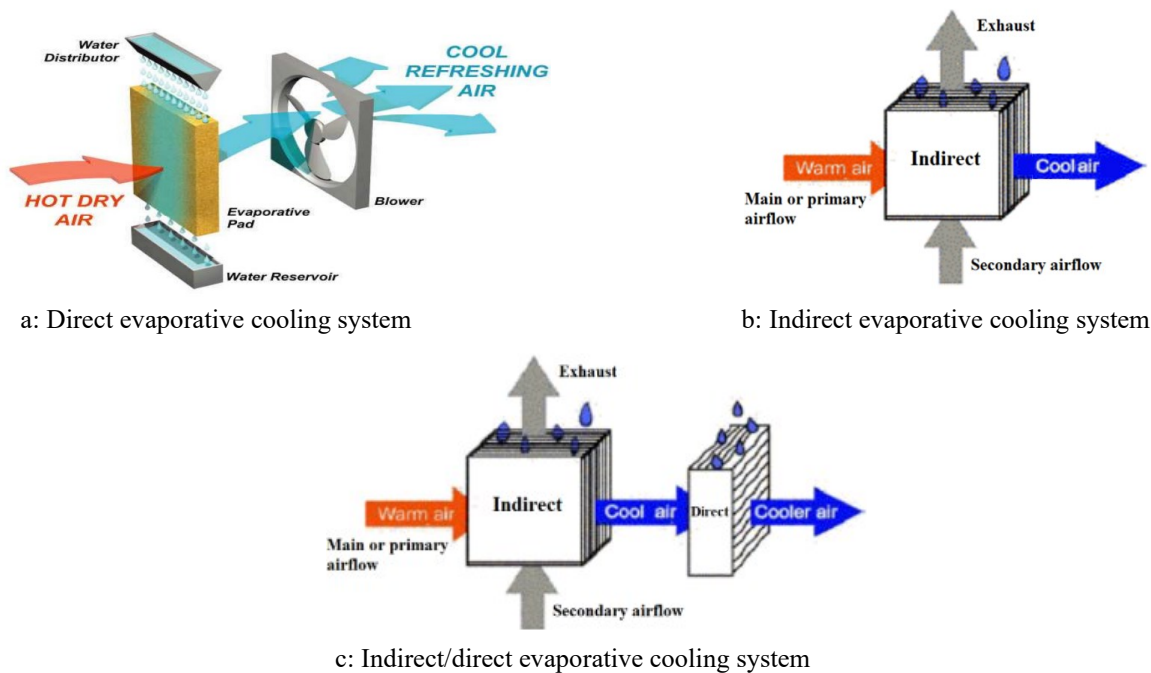


Figure 1. Types of evaporative cooling systems (Musa, 2009).



As a result, the heat is dissipated from the exterior airflow as it passes over the cool surface, consequently, air flows out of the system at a low temperature (Yan, 2017). The third type of evaporative cooling system is a hybrid between the first two types; in this type, the airflow is cooled sensibly by passing it through an indirect evaporative cooling system, then being further cooled by passing it through wet cellulose pads in a direct evaporative cooling system (Musa, 2009).

Many researchers have numerically and experimentally investigated the effectiveness of evaporative cooling systems of all types in improving indoor thermal conditions in buildings for multiple residential, agricultural, and industrial applications. (Alhosainy and Aljubury, 2019) studied experimentally the impact of using a two-stage evaporative cooling system in improving the thermal comfort of the domestic room. The utilized cooling system included two heat exchangers in the indirect cooling stage and three cellulosic pads with a thickness of three cm for each pad in the direct cooling stage. The experiments were carried out under the climatic conditions of Baghdad City during the summertime of 2018 (starting from July to October). The researchers used underground water as a working fluid in the proposed cooling system, at 5 Lpm in both heat exchangers and 4.5 Lpm in the cellulosic pads. The experimental outcomes showed that the system's total efficiency reached 167% with a difference in temperature of 26.2 °C between the ambient and the supply air when using two heat exchangers in the indirect cooling stage, and when using one heat exchanger the efficiency decreased to 122.7% with a difference in temperature of 16 °C between the ambient and supply air. Moreover, the total efficiency decreased to 84.36 % when using only the direct cooling stage (i.e., when using a direct evaporative cooling system). (Ali and Albayati, 2017) experimentally studied the use of two techniques to cope with the problem of overheating air temperature inside the greenhouse. The first technique comprised using shading with various configurations ranging from shade-1 to shade-4, and the second technique was utilizing a two-stage evaporative cooler. The utilized evaporative cooler involved a heat exchanger in the indirect cooling stage and three cellulosic pads with a thickness of 3 cm for each pad in the direct cooling stage. The experimental work was conducted under the climatic conditions of Baghdad City. The experimental findings showed that the evaporative cooler contributed to increasing the humidity level inside the greenhouse, where the percentage of the increment in humidity ranged between 562.5 and 871 depending on the type of the used shading configuration.

In the same context, (Aljubury and Ridha, 2017) studied experimentally the effect of using an Indirect/direct evaporative cooling system on enhancing thermal conditions inside the greenhouse. The cooling system consisted of one heat exchanger in the indirect cooling stage and three cellulosic pads with a thickness of 3 cm for each pad in the direct cooling stage. The underground water was used as an operating fluid in the proposed cooling system, at 2 L/s in the heat exchanger of the indirect cooling stage and 3 L/s in the cellulose pads of the direct cooling stage. The experiments were conducted throughout the summer months of 2015 (July through August) in Baghdad City. The experimental outcomes revealed that using the indirect/direct evaporative cooling system led to an increase in the system efficiency of up to 108% compared to the efficiency of the direct evaporative cooling system which reached 77.5%. (Kowalski and Kwiecien, 2020) employed (TRNSYS 17) software to evaluate the role of an evaporative cooling system in enhancing the indoor thermal environment of industrial buildings in Poland's climate. The analysis included the assessment of both types of evaporative cooling systems (i.e., the direct and indirect cooling systems) in terms of coefficient of performance based on the season, water and electricity consumption, and the duration of time during which each system fails to reach the desired

room air temperature setpoint (TTF). The results of the study suggested that utilizing evaporative cooling systems in Poland could decrease energy consumption. Furthermore, the research revealed that the use of both direct and indirect evaporative cooling systems has significant potential for application in the climate of Poland. (Moran et al., 2021) used a combination of modelling and experimental approaches to investigate the impact of different techniques on enhancing thermal comfort inside shelters located in a desert refugee camp. The researchers constructed a laboratory prototype made up of 12 shelters and conducted various tests and simulations on them to assess the overall thermal conditions of shelters. The proposed techniques comprised placing solar panels over the roof of lab shelters, as well as installing evaporative coolers in them to provide the required cooling load. The study outcomes showed that the desert evaporative cooler proved to be the most efficient system in mitigating interior peak temperatures by around 5.8 degrees Celsius. Nevertheless, the researchers indicated that despite these devices being powered by photovoltaic (PV) panels and not relying on the camp's power sources, they still consume water at a rate of 0.6 liters per hour. Consequently, the widespread adoption of such equipment may potentially lead to an increase in water demand inside the camp.

The use of indirect/direct evaporative cooling systems to provide thermally acceptable conditions in relief tents is a comparatively fresh field of study. This cooling technique is still in its earliest stages and requires further investigation. Therefore, as an alternative to the conventional single-stage direct evaporative cooling system, the present study aims to illustrate a numerical assessment of the feasibility of using an indirect/direct evaporative cooling system that involves two heat exchangers in its indirect cooling stage to enhance the interior thermal environment of the relief tent.

The proposed indirect/direct evaporative cooling system (as shown in Fig. 2) is based on sensible and latent heat exchange within the indirect and direct stages to reduce the outlet air temperature from the cooling system. Heat exchangers are utilized to chill the air sensibly,

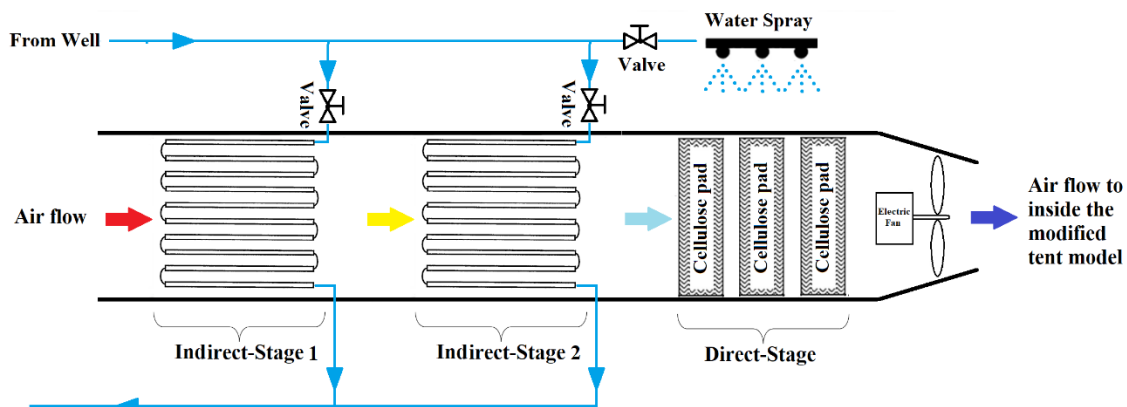


Figure 2. Schematic diagram of the proposed evaporative cooling system.

whereas cellulosic pads are utilized to chill the air sensibly and increase the moisture content at the same time. Fig. 3 explains the principle of the processes within the proposed cooling system. The warm air (point 1) flows inside the dry channels of the first heat exchanger and loses part of its heat to the wet channels, consequently, the outlet air from the first heat exchanger (point 2) will have a lower temperature than the inlet air. Then, the airflow temperature is reduced further when air flows through the second heat exchanger (point 2 to point 3). The airflow, after that, flows through the wet cellulosic pads, where

sensible-latent heat exchange between the air and water in these pads is done, thus, the air temperature at the pads' outlet (point 4) drops with increasing its moisture content as well.

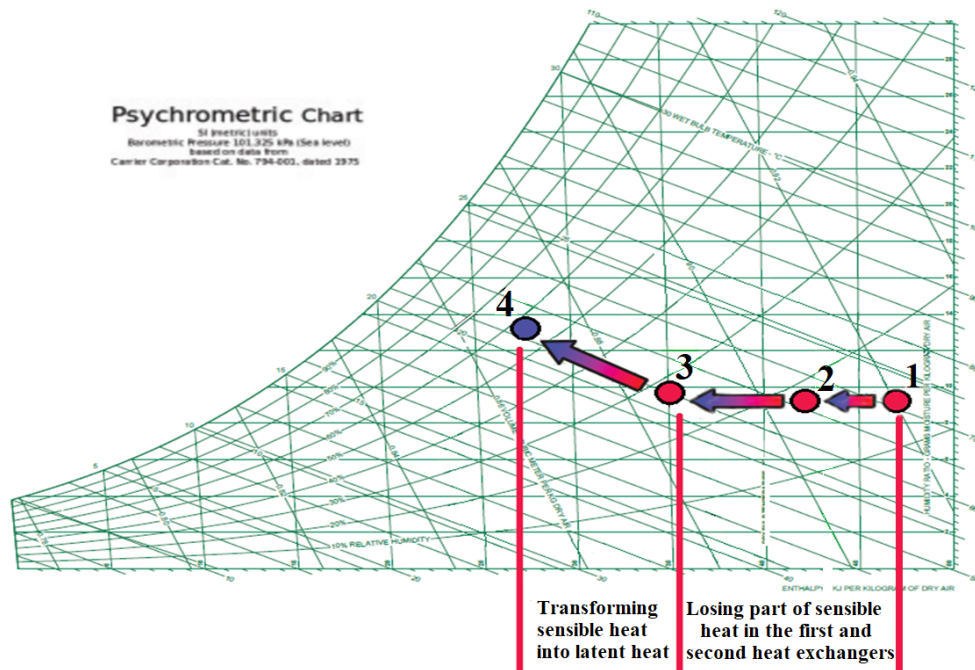


Figure 3. Principle of proposed evaporative cooling system on the Psychrometric chart.

2. METHODOLOGY

2.1 Numerical Part

The computational fluid dynamics (CFD) approach was originally intended as a modelling tool for testing and evaluating mechanical systems, but it was used later in construction-related fields for evaluating both the buildings' interior and outside environments, as well as the effect they have on the building's envelope (Erell et al., 2012). The main advantage of (CFD) techniques is that they can be utilized to assess a variety of factors that affect the interior and exterior environments of the buildings, such as the air state and its speed and movement, the spread of airborne pollutants, thermal comfort conditions, as well as the relative humidity (Blocken and Persoon, 2009; Tominaga and Stathopoulos, 2009; Chung and Choo, 2011). As indicated in Fig. 4a, the geometry of the problem under investigation is described and shown in the physical domain. The geometry is a three-dimensional model of a Standard Emergency Relief Tent with dimensions of (5680×3320×2830 mm). The present study's meshed case, as illustrated in Fig. 4b, was created by using software written in FORTRAN. At the nodes of each cell, the solutions to the flow field issues (temperature, relative humidity and velocity of air, as well as the PMV) were defined.

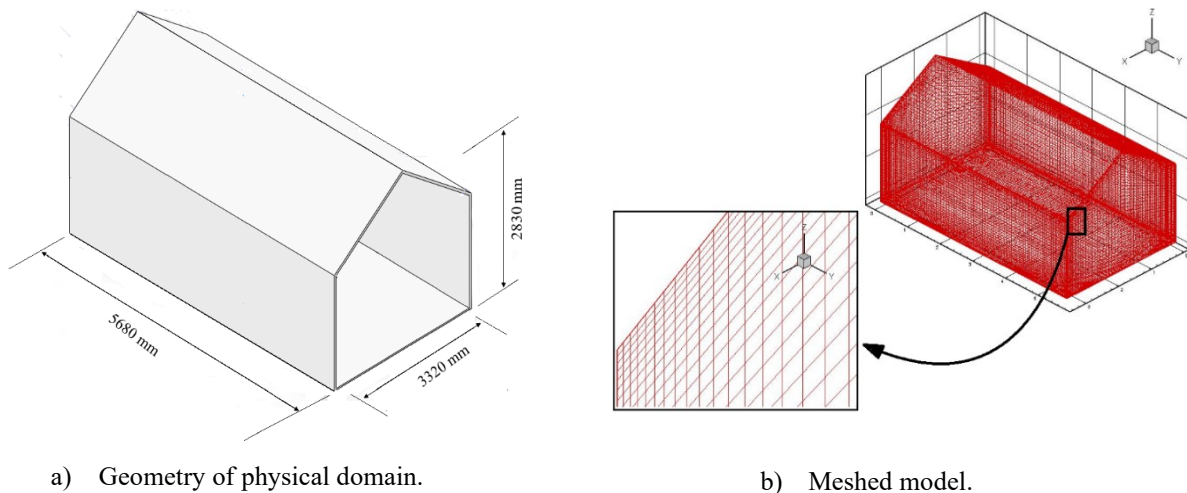


Figure 4. Schematic diagram of the studied case.

Moreover, to ensure that the grid meets the best possible quality, the independence of the grid has been checked by carrying out a mesh independence test. As indicated in **Table 1**, several grid sizes were used for the grid independence test while maintaining a fixed number of elements in the z-direction. The convergence limits used for the test were 1×10^{-6} . The results of the test as depicted in **Fig. 5**, showed that the inner zone temperature at the grid size of 300000 varied very slightly compared with the temperature that was achieved at the grid size of 360000. Therefore, this grid size was adopted in all numerical analyses. The numerical analysis was conducted after applying different assumptions, namely: the case study was assumed to be unsteady three-dimensional, the airflow through the tent model was considered to be turbulent incompressible flow, and the thermophysical parameters of the airflow were assumed to be constant. The impact of various parameters, including the cellulose pad thickness and the volumetric water flow rates in the second heat exchanger of the indirect cooling stage on the thermal performance of the proposed cooling system was analyzed, where the tested values of pad thickness were 10 and 15 cm. The rates of water flow were 2 and 4 Lpm. The underground water was assumed to be pumped into the system via an electric pump driven by PV panels.

Table 1. Mesh independence test’s outcomes.

Grid size (x, y, z)	Number of elements	The temperature of the interior zone (°C)	Error percentage (%)
60×50×40	120000	42.546	3.951018
60×50×60	180000	40.865	2.904686
60×50×80	240000	39.678	2.021271
60×50×100	300000	38.876	0.231505
60×50×120	360000	38.786	

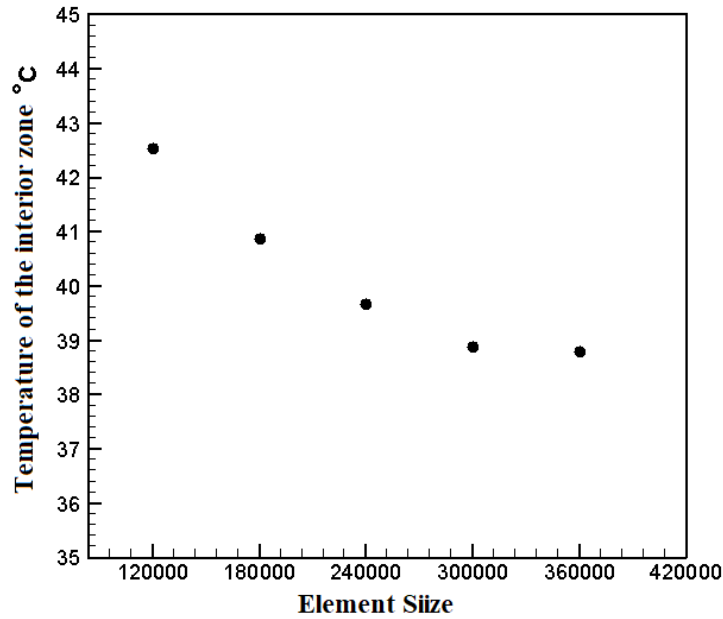


Figure 5. Mesh independence test's outcomes.

Depending on the properties of the flow, the physical phenomenon can be described by choosing the appropriate set of equations. Therefore, in the present study, the governing equations, including continuity, momentum, energy, and transport equations for turbulence, were used in Cartesian coordinates as follows (Mays, 2021):

- **Continuity equation:**

$$\frac{\partial \rho}{\partial t} + \frac{\partial}{\partial x} \rho u + \frac{\partial}{\partial y} \rho v + \frac{\partial}{\partial z} \rho w = 0 \tag{1}$$

Where the terms u, v, and w represent the velocity components corresponding to the cartesian coordinates.

Momentum equation in x-direction:

$$\rho \frac{\partial U}{\partial \tau} + \rho U \frac{\partial U}{\partial X} + \rho V \frac{\partial U}{\partial Y} + \rho W \frac{\partial U}{\partial Z} = -\frac{\partial P}{\partial X} + \frac{\partial}{\partial X} [(\mu + \mu_t) (2 \frac{\partial U}{\partial X})] + \frac{\partial}{\partial Y} [(\mu + \mu_t) (\frac{\partial U}{\partial Y} + \frac{\partial V}{\partial X})] + \frac{\partial}{\partial Z} [(\mu + \mu_t) (\frac{\partial U}{\partial Z} + \frac{\partial W}{\partial X})] \tag{2}$$

Momentum equation in y-direction:

$$\rho \frac{\partial V}{\partial \tau} + \rho U \frac{\partial V}{\partial X} + \rho V \frac{\partial V}{\partial Y} + \rho W \frac{\partial V}{\partial Z} = -\frac{\partial P}{\partial Y} + [(\mu + \mu_t) (\frac{\partial V}{\partial X} + \frac{\partial U}{\partial Y})] + \frac{\partial}{\partial Y} [(\mu + \mu_t) (\frac{\partial V}{\partial Y} + \frac{\partial V}{\partial Y})] + \frac{\partial}{\partial Z} [(\mu + \mu_t) (\frac{\partial V}{\partial Z} + \frac{\partial W}{\partial Y})] + \rho g \beta_T (T - T_o) + \rho g \beta_c (C - C_o) \tag{3}$$

Momentum equation in z-direction:

$$\rho \frac{\partial W}{\partial \tau} + \rho U \frac{\partial W}{\partial X} + \rho V \frac{\partial W}{\partial Y} + \rho W \frac{\partial W}{\partial Z} = -\frac{\partial P}{\partial Z} + \frac{\partial}{\partial X} [(\mu + \mu_t) (\frac{\partial W}{\partial X} + \frac{\partial U}{\partial Z})] + \frac{\partial}{\partial Y} [(\mu + \mu_t) (\frac{\partial W}{\partial Y} + \frac{\partial V}{\partial Z})] + \frac{\partial}{\partial Z} [(\mu + \mu_t) (2 \frac{\partial W}{\partial Z})] \tag{4}$$



Energy equation:

$$\rho \frac{\partial T}{\partial \tau} + \rho U \frac{\partial T}{\partial X} + \rho V \frac{\partial T}{\partial Y} + \rho W \frac{\partial T}{\partial Z} = \frac{\partial}{\partial X} \left[\left(\frac{\mu}{\rho_r} + \frac{\mu_t}{\sigma_T} \right) \left(\frac{\partial T}{\partial X} \right) \right] + \frac{\partial}{\partial Y} \left[\left(\frac{\mu}{\rho_r} + \frac{\mu_t}{\sigma_T} \right) \left(\frac{\partial T}{\partial Y} \right) \right] + \frac{\partial}{\partial Z} \left[\left(\frac{\mu}{\rho_r} + \frac{\mu_t}{\sigma_T} \right) \left(\frac{\partial T}{\partial Z} \right) \right] \quad (5)$$

Conduction Equation:

$$\frac{\partial T}{\partial x} = \frac{\mu c_p}{k} \left[\frac{\partial}{\partial x} \left(\frac{\partial T}{\partial x} \right) + \frac{\partial}{\partial y} \left(\frac{\partial T}{\partial z} \right) + \frac{\partial y}{\partial x} \left(\frac{\partial T}{\partial z} \right) \right] \quad (6)$$

- **Transport equation of turbulence:**

The low Reynolds (k-ε) model used in this investigation is based on turbulence kinetic and dissipation equations, which are described below:

- **Turbulence kinetic energy equation (K):**

$$\rho \frac{\partial K}{\partial \tau} + \rho U \frac{\partial K}{\partial X} + \rho V \frac{\partial K}{\partial Y} + \rho W \frac{\partial K}{\partial Z} = \frac{\partial}{\partial X} \left[\left(\mu + \frac{\mu_t}{\sigma_k} \right) \left(\frac{\partial K}{\partial X} \right) \right] + \frac{\partial}{\partial Y} \left[\left(\mu + \frac{\mu_t}{\sigma_k} \right) \left(\frac{\partial K}{\partial Y} \right) \right] + \frac{\partial}{\partial Z} \left[\left(\mu + \frac{\mu_t}{\sigma_k} \right) \left(\frac{\partial K}{\partial Z} \right) \right] - D + G_k - \rho \epsilon \quad (7)$$

Turbulence dissipation equation (ε) :

$$\rho \frac{\partial \epsilon}{\partial \tau} + \rho U \frac{\partial \epsilon}{\partial X} + \rho V \frac{\partial \epsilon}{\partial Y} + \rho W \frac{\partial \epsilon}{\partial Z} = \frac{\partial}{\partial X} \left[\left(\mu + \frac{\mu_t}{\sigma_\epsilon} \right) \left(\frac{\partial \epsilon}{\partial X} \right) \right] + \frac{\partial}{\partial Y} \left[\left(\mu + \frac{\mu_t}{\sigma_\epsilon} \right) \left(\frac{\partial \epsilon}{\partial Y} \right) \right] + \frac{\partial}{\partial Z} \left[\left(\mu + \frac{\mu_t}{\sigma_\epsilon} \right) \left(\frac{\partial \epsilon}{\partial Z} \right) \right] + C_{\epsilon 1} f_1 \frac{\epsilon}{k} G_k + C_{\epsilon 2} f_2 \rho \frac{\epsilon^2}{k} + E \quad (8)$$

The values of the constants ($C_\mu, C_{\epsilon 1}, C_{\epsilon 2}, \sigma_k, \sigma_\epsilon$) in Eq.s (7 and 8) were adopted from reference (Jagadeesh and Murali, 2005) and presented in **Table 2**.

Table 2. Values of the constants that emerged in turbulent transport equations.

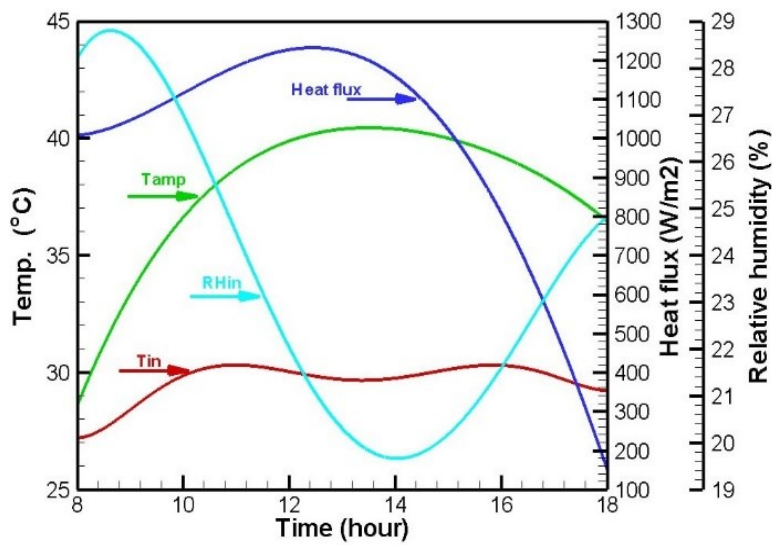
C_μ	$C_{\epsilon 1}$	$C_{\epsilon 2}$	$C_{\epsilon 3}$	σ_k	σ_ϵ	$\sigma_T = \sigma_C$
0.09	1.44	1.92	Tanh[V/U]	1.0	1.30`	0.9

An initial estimate is needed to create the solution since the flow field cannot be calculated without starting an iteration. The initialization of the model affects convergence, and if the initial conditions are poorly stated, the solution will take longer to converge or may even diverge. Moreover, stating clear boundary conditions for the studied model will produce a precise solution. Based on the above, the initial and boundary conditions were included in **Table 3**. The boundary conditions were selected to match the experimental data obtained on certain days over the summer of 2022 (more precisely, from July 15th to September 15th).

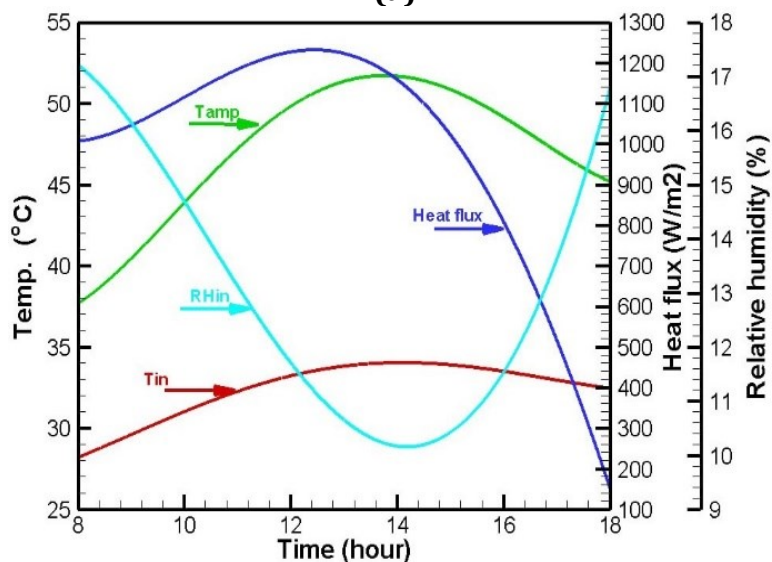


Table 3. Initial and boundary conditions

Initial conditions	$T_{Interior, zone}$	The value is changeable with time (from experimental data, see Fig. 6.)
	$RH_{Interior, zone}$	The value is changeable with time (from experimental data, see Fig. 6.)
Boundary conditions	Inlet	$u=6.46$ m/s (min.), and 8.54 m/s (max.)
		$k = V_{in}^2 \times I^2$, where $I=0.16 \times u_{in} \times D_h / \mu$
		$\epsilon = C_{\mu}^{0.75} \times k^{1.5} / 0.07 D_h$
	Outlet	$\frac{\partial u}{\partial x} = \frac{\partial v}{\partial x} = \frac{\partial w}{\partial x} = \frac{\partial k}{\partial x} = \frac{\partial \epsilon}{\partial x} = \frac{\partial T}{\partial x} = 0$
At the walls	$u=v=w=0$	
		Solar flux and $T_{ambient}$ are changeable with time (from experimental data, see Fig. 6.)



(a)



(b)

Figure 6. Experimental data that were used as initial and boundary conditions, (a) at 25/8/2022, (b) at 3/9/2022.



The numerical calculations in the Fortran program are done according to the following approach: The grid generation process involves utilizing algebraic equations to obtain the desired form. Subsequently, the governing equations are converted from Cartesian coordinates to general coordinates. Following this transformation, the initial and boundary conditions are applied within the program to compute the velocity equations (U, V, W) in the three directions. This is achieved by converting complex differential equations into simpler algebraic equations. The LSOR method is employed to solve these equations, while the Tridiagonal matrix method is utilized for matrix solutions. Additionally, the pressure values are calculated using the SIMPLE algorithm method. The equations for Turbulent Kinetic Energy and the Rate of Energy Dissipation are computed using the same procedure as the velocity solution. The determination of viscosity values under turbulent conditions involves the use of the computed Turbulent Kinetic Energy (TKE) and the rate of energy dissipation. The temperature equation is computed using the same procedure as the preceding one.

2.2 Validation of the Numerical Model

Figs. 7 and 8 show the validation of the tent model's numerical results with the experimental data in terms of matching the data of indoor air temperature distribution under the following conditions: airflow at low speed, pad thicknesses of 10 and 15 cm, volumetric water flow rate of 3 Lpm in the first heat exchanger of the indirect cooling stage as well as in the cellulose pad, and a variable volumetric water flow rate of 2, and 4 lpm in the second heat exchanger. It is clear that the numerical findings match well with the experimental data.

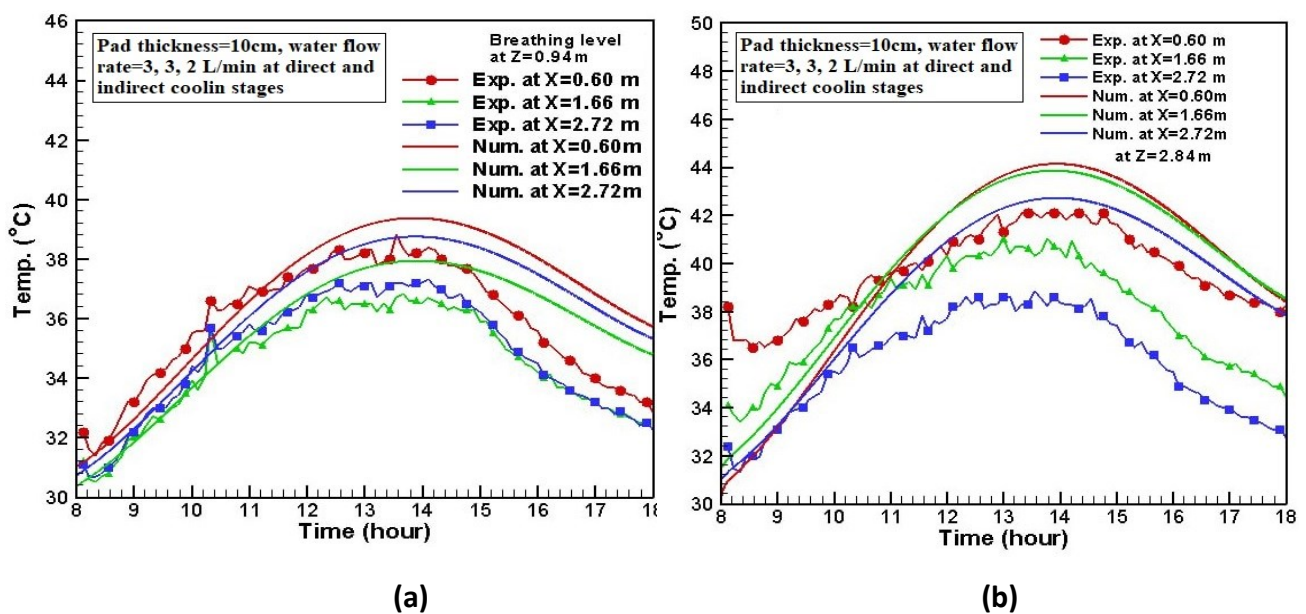


Figure 7. Validation of the numerical model with the experimental data in terms of temperature distribution vs. the time, at one pad of 10 cm, a water flow rate of (3, 3, and 2) lpm in the direct, first, and second coils indirect stages, respectively, (a) at Z=0.94 m, (b) at Z= 2.84 m.

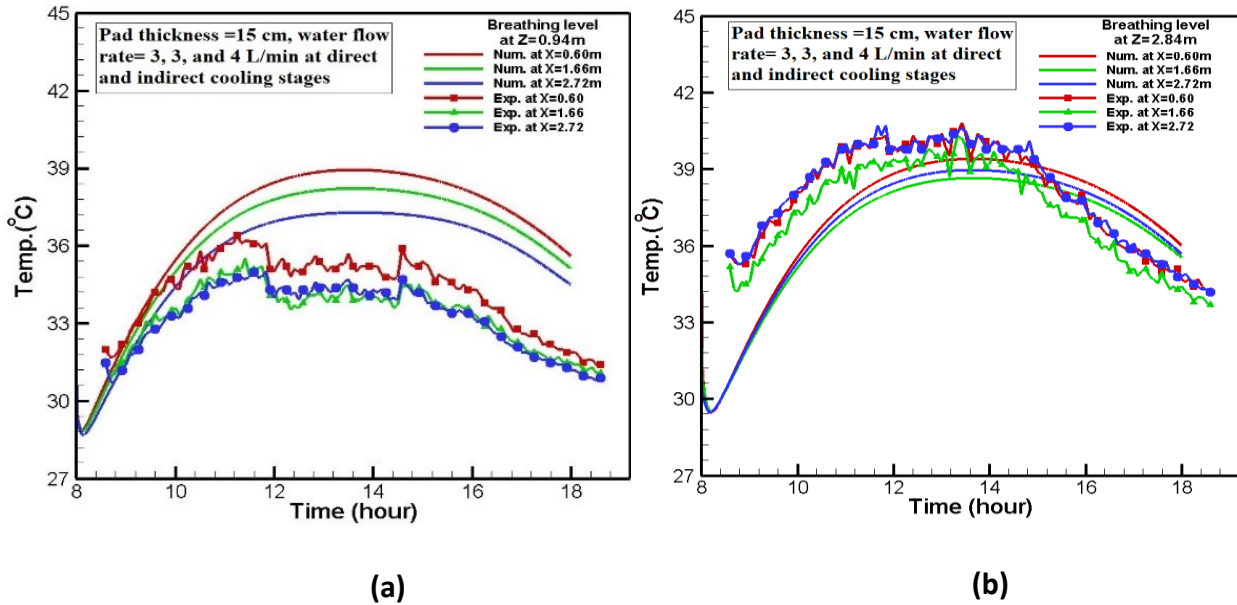


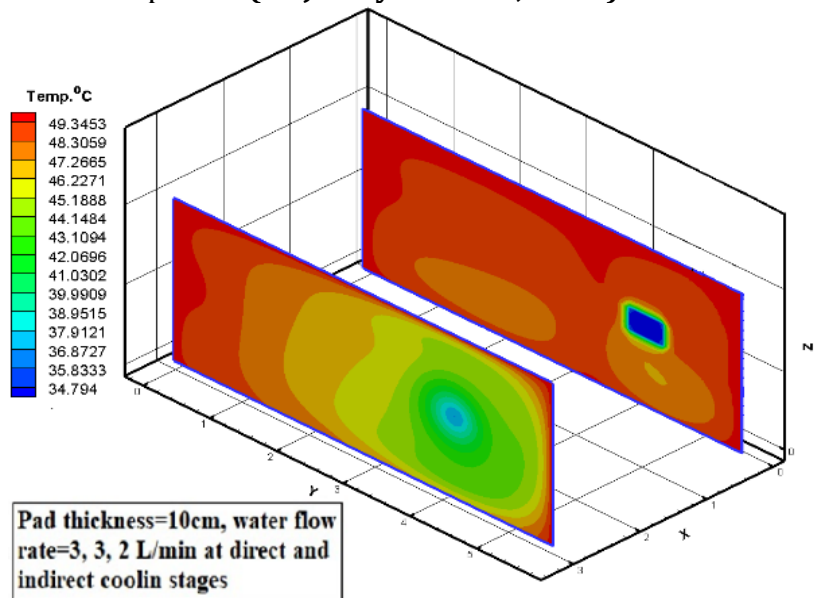
Figure 8. Validation of the numerical model with the experimental data in terms of temperature distribution vs. the time, at one pad of 15 cm, a water flow rate of (3, 3, and 4) lpm in the direct, first, and second coils indirect stages, respectively, (a) at $Z=0.94$ m, (b) at $Z= 2.84$ m.

3. RESULTS AND DISCUSSION

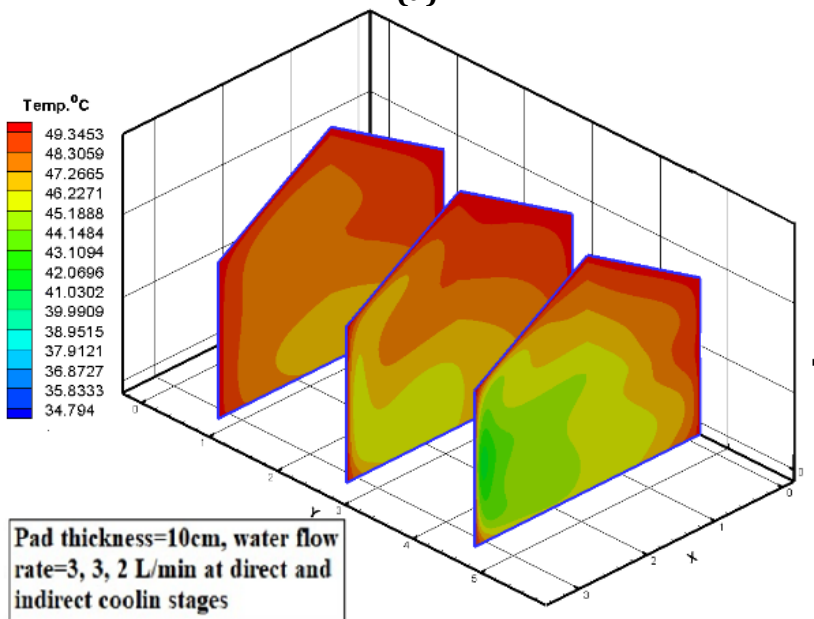
Figs. 9 and 10 show the temperature distribution within the modified tent model along the tent's longitudinal axis during the peak hour, at pad thicknesses of 10 and 15 cm and various water flow rates in the cooling system stages. According to these figures, the first section of the tent, which is located closest to the air supply entrance of the cooling system has the lowest temperatures because the airflow there is disturbed by vortices which are caused by mixing the indoor air with the cold air who flows from the supply entrance at a high speed, and as the airflow moves towards the other side of the tent, the effect of these vortices diminishes, and the airflow return to flow in smooth streamlines, consequently, the mixing rate with the interior air slows down. Hence, as the air moves towards the tent's end, its temperature will increase due to the gradual loss of heat from the surrounding hot air to airflow.

It is important to indicate that the existence of two heat exchangers in the indirect cooling stage of the cooling system contributes to maintaining a thermally comfortable environment inside the tent model and this exceptional performance of the proposed cooling system in reducing the temperature inside the tent may be attributed to further decrease in both dry and wet bulb air temperatures when passing through the heat exchangers prior to entering the direct cooling stage (**Mohammed and Mohammed, 2013**). In addition, it can be noted from these Figures, that when increasing the cellulose pad thickness to 15 cm with raising the water flow rate in the second heat exchanger from 2 to 4 Lpm, the reduction in indoor temperatures increased by about 19%. This result could be attributed to two interpretations: The first one is, that increasing the cellulose pad thickness will result in an increase in the internal heat transfer surface area, which in turn will result in an increase in the rate of heat exchange between the airflow and the wet contact surfaces (**Faisal et al.,**

1997), while the second interpretation is that, the thermal resistance created by the heat exchanger's tube walls and the associated fouling on both sides of the tubes slow down the pace at which heat is transferred from the airflow to the water in the heat exchanger. Therefore, the volume of water flowing through the tubes determines the amount of thermal energy extracted from the air stream; and as the volume of water flow increases, the impact of thermal resistance gets smaller and the value of the heat transfer coefficient within the heat exchanger's tubes improves (Al-Juwayhel et al., 2004).

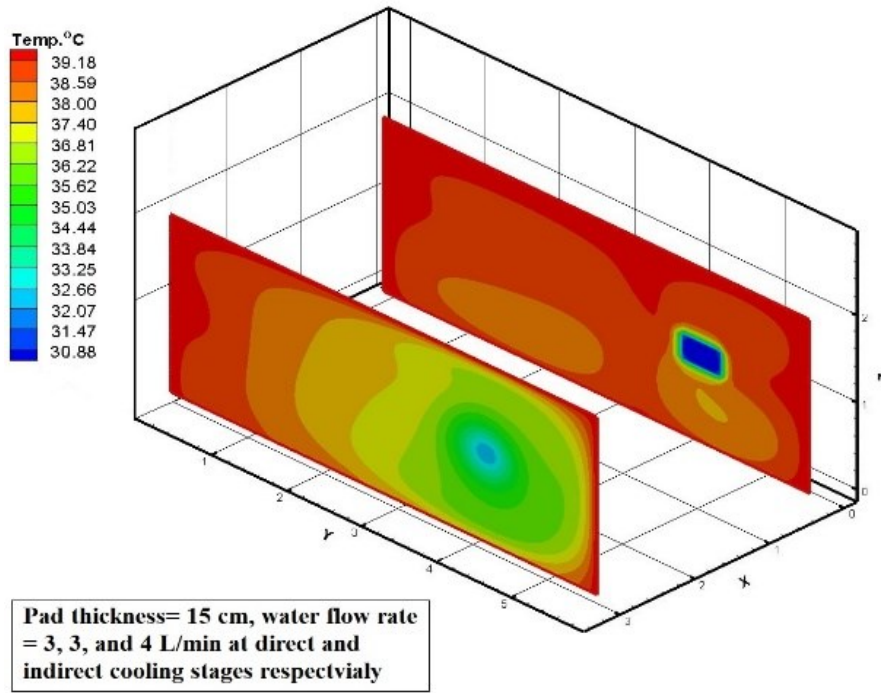


(a)

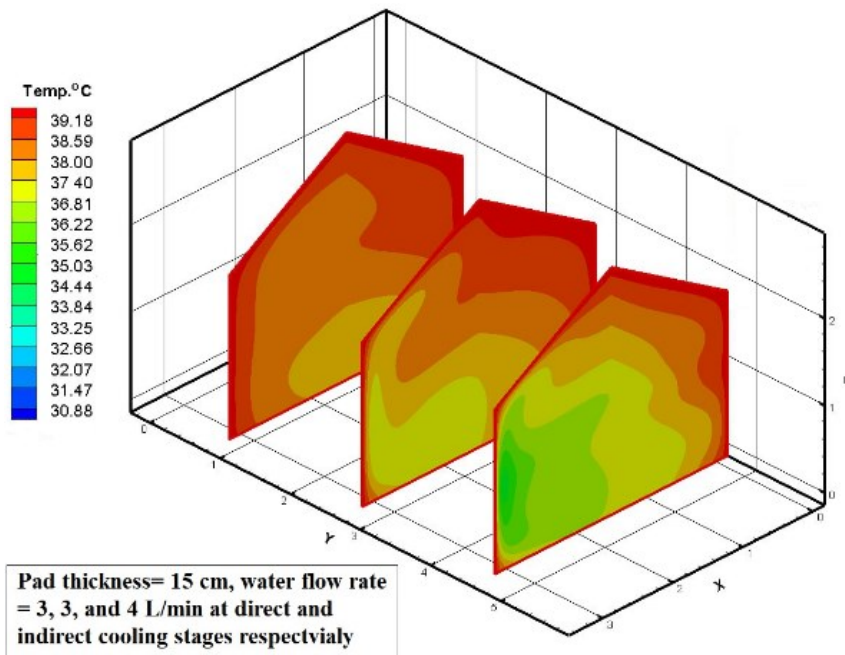


(b)

Figure 9: Temperature distribution inside the modified tent model along the tent's longitudinal axis at peak hour, one pad with 10 cm thickness, water flow rate of (3, 3, and 2) Lpm in the direct stage, first, and second coils of indirect stage, respectively, (a) Distribution along the Y-axis, (b) Distribution along the x-axis.



(a)



(b)

Figure 10. Temperature distribution inside the modified tent model along its axis at peak hour, one pad with 15 cm thickness, the water flow rate of (3, 3, and 4) lpm in the direct stage, first, and second coils of the indirect stage, respectively, (a) Distribution along the Y-axis, (b) Distribution along the x-axis.

Figs. 11 and 12 show the relative humidity distribution within the modified tent model during peak hours with the tent's longitudinal axis. The pad thicknesses of 10 and 15 cm and at a constant flow rate of 3 lpm in the direct cooling stage as well as in the first heat exchanger of the indirect cooling stage, while the water flow rate in the second heat exchanger was variable. As shown in these Figures, the first section of the tent, which is the closest to the cooling system's air supply entrance, has the maximum relative humidity due to an increase in mass transfer between the humid air flowing from the supply entrance and the interior air, because of the high levels of turbulence caused by the formation of vortices when the humid airflow enters the supply entrance at a high velocity and merges with the tent's interior air. Moreover, the impact of these vortices lessens as the airflow moves toward the end of the tent and resumes flow in smooth streamlines. As a result, the mixing rate with the interior air lowers (i.e., the rate of mass transfer from the airflow into the rest of the ambient air reduces in these zones).

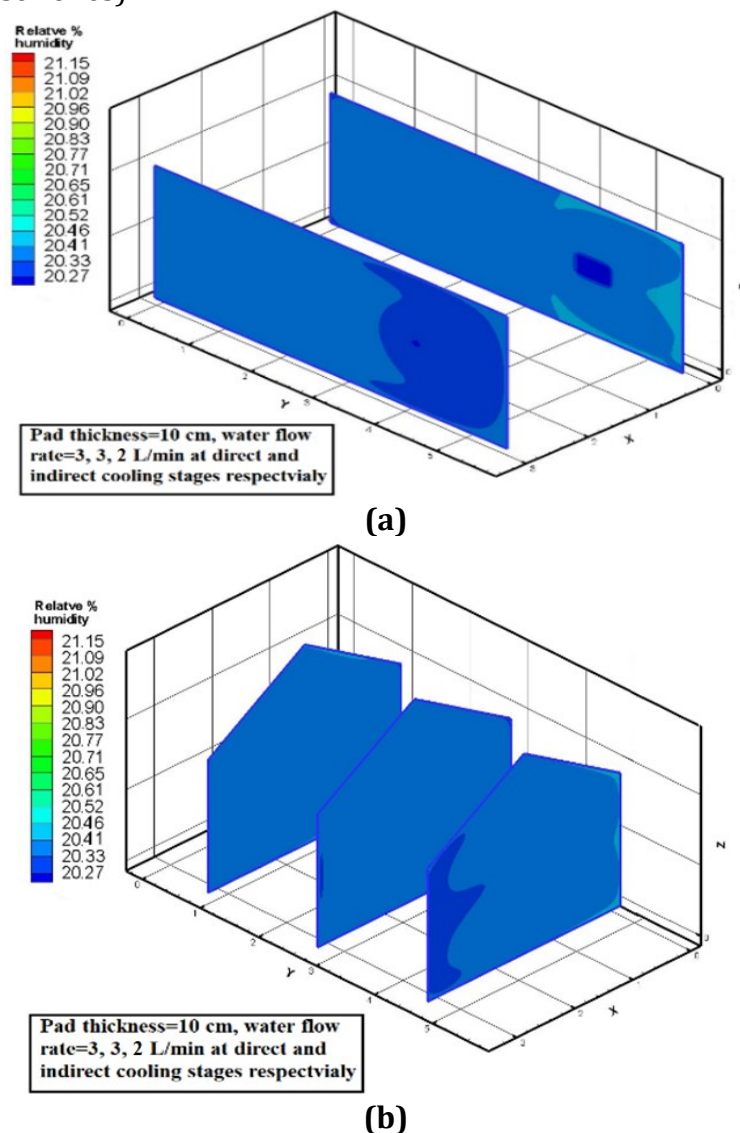
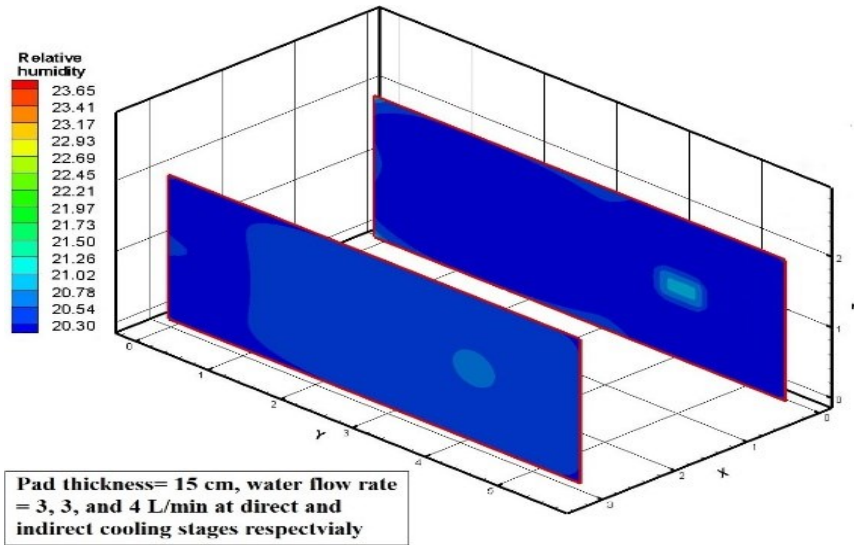
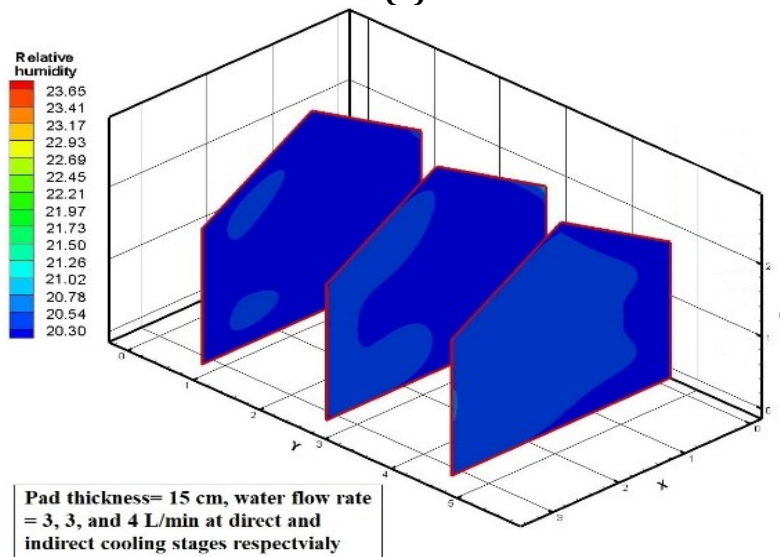


Figure 11. Relative humidity distribution inside the modified tent model along the tent's longitudinal axis at peak hour, one pad with 10 cm thickness, a water flow rate of (3, 3, and 2) Lpm in the direct stage, first, and second coils of indirect stage, respectively, (a) Distribution along the Y-axis, (b) Distribution along the X-axis.



(a)



(b)

Figure 12. Relative humidity distribution inside the modified tent model along the tent's longitudinal axis at peak hour, one pad with 15 cm thickness, a water flow rate of (3, 3, and 4) lpm in the direct stage, first, and second coils of the indirect stage, respectively, (a) Distribution along the Y-axis, (b) Distribution along the x-axis.

Fig. 13 shows the air velocity vector distribution along the longitudinal axis of the modified tent model, at different cellulosic pad thicknesses of 10 and 15 cm and at a constant water flow rate of 3 Lpm in the direct cooling stage as well as in the first heat exchanger of the indirect cooling stage, while the water flow rate in the second heat exchanger was variable. This figure illustrates that the magnitude of air velocity vectors rises in the area near the cooling system's air supply hole due to mutual turbulence caused by the vortices that are formed there as a result of speedily air flowing from the supply entrance (**Tan and Tan, 2021**). Additionally, when the airflow goes away from the supply hole and toward the tent end, the impact of vortices decreases as the air begins moving in smooth streamlines.

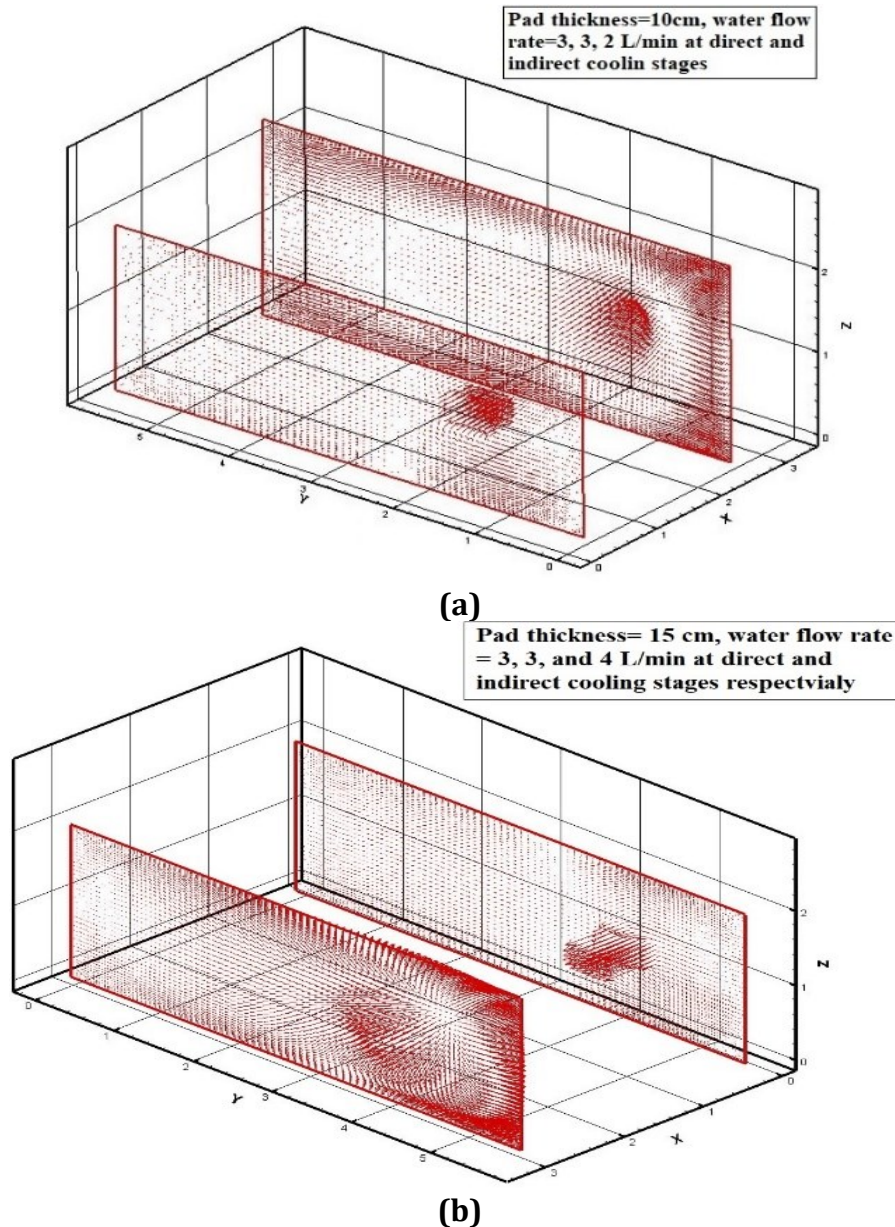


Figure 13: Velocity vector distribution inside the modified tent model along the tent's longitudinal axis at peak hour, at different pad thicknesses, and water flow rate of (2, and 4) lpm in the second heat exchanger of the indirect cooling stage, (a) at pad thickness =10cm, (b) at pad thickness =15 cm.

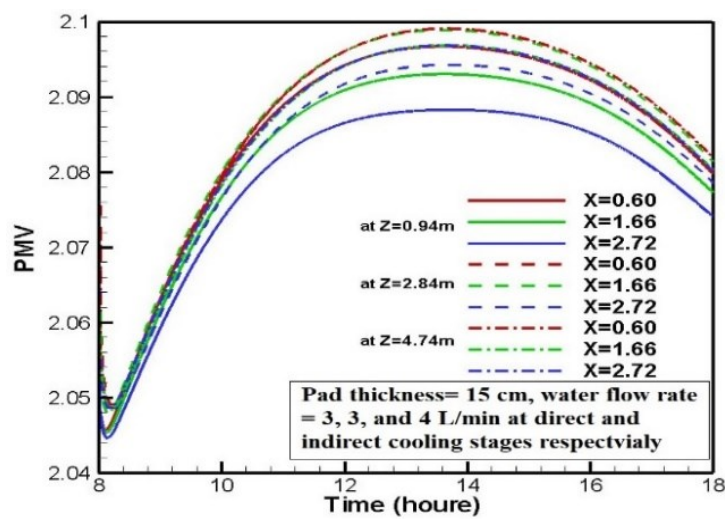
Predicted Mean Vote (PMV) which was presented by **(Fanger, 1970)**, may be utilized for predicting thermal performance within the tent model. The PMV can be calculated using six environmental physical parameters namely air temperature and how it moves, relative humidity level, mean radiant temperature, metabolism rate, and degree of thermal insulating for clothes **(Susanti, 2015)**. As indicated in **Table 4.**, the PMV value may be separated into different stages ranging from -3 to +3. When the PMV number reaches to +3, the thermal comfort (i.e., the interior environment) is the hottest. While, when the PMV number reaches -3, the thermal comfort (the interior environment) is the coldest. Thermal comfort is considered to be moderate if the score is 0 **(Karyono et al., 2020)**.



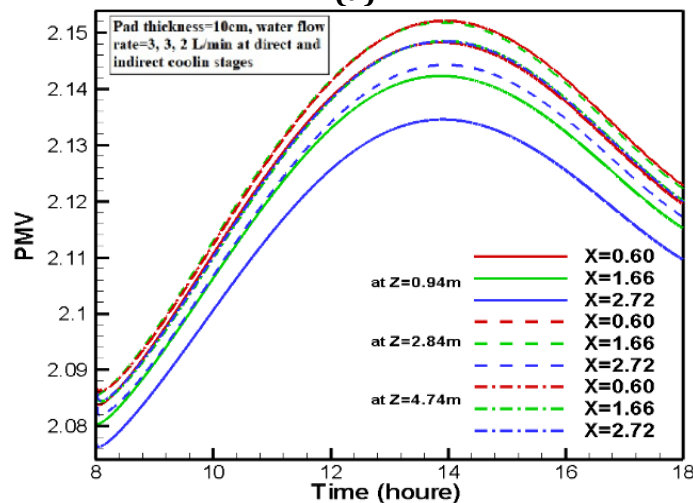
Table 4. ASHRAE's thermal sensation vote scale

PMV	+3	+2	+1	0	-1	-2	-3
Thermal Sensation	Hot	Warm	Slightly warm	Neutral	Slightly Cool	Cool	Cold

Fig. 14 presented the PMV distribution versus the time to observe how the PMV varies at different particular locations within the tent model when using different cellulose pad thicknesses of 10 and 15 cm and different water flow rates of 2 and 4 Lpm in the second heat exchanger of the indirect cooling stage. As shown in this Figure, the PMV values are within the ASHRAE's thermal sensation vote scale, which means the thermal comfort (i.e., interior environment) is cool. Moreover, Thermal PMV values are at a low level in the early hours of the day and reach the maximum level at noon because of increasing the outdoor air temperature.



(a)



(b)

Figure 14. PMV distribution inside the modified tent model, at different pad thicknesses, and water flow rate of (2, and 4) lpm in the second heat exchanger of the indirect cooling stage, (a) at pad thickness =15cm, (b) at pad thickness =10 cm.



4. CONCLUSIONS

The internal thermal conditions of tents, tend to be higher during the daytime compared to the exterior temperature. Conversely, in the late afternoon or evening, the interior thermal condition is cooler than the temperature outside. These fluctuations have a detrimental impact on the degree of comfort experienced by the occupants of the tents. Therefore, it is essential to use an appropriate technology, which in the case of the present work is an indirect/direct evaporative cooling system, to address this issue with the aim of enhancing the inside thermal comfort conditions of tents. Several important results were reached, which are summarized in the following points:

- 1- The two-stage indirect/direct cooling system contributes to maintaining a thermally comfortable environment within the tent model because of the effective performance of the heat exchangers of the indirect cooling stage in reducing the dry and wet bulb temperatures of the airflow before entering into the direct evaporative cooling stage.
- 2- Due to the high effectiveness of the two heat exchangers of the indirect cooling stage in achieving thermal comfort inside the modified tent model, it is feasible to improve the thermal comfort inside the modified tent model even if the cooling system is used without the (direct evaporative cooling stage).
- 3- Thermal comfort conditions improve in conjunction with increasing both the thickness of the cellulose pad and the elevation of water volume flow rates in the heat exchangers of the indirect cooling stage, where the drop in interior temperature increased by about 19% when increasing the thickness to 15 cm and raising the water flow rate to 4 Lpm respectively.
- 4- The Predicted Mean Vote (PMV) values which are normally utilized to predict the thermal performance within the tent model are within the ASHRAE's thermal sensation vote scale, which means the obtainable thermal comfort in case of applying the proposed evaporative cooling system is in the acceptable range.

NOMENCLATURE

Symbol	Description	Symbol	Description
D	Used value for low (Re) turbulence models are utilized	t	Time (s)
E	A term made when low (Re) turbulence models are utilized	u, v, w	Cartesian coordinate-corresponding velocity components (m/s)
G_k	turbulent energy production generated by the buoyancy forces, $G_K = - \frac{\mu_t}{\sigma_T} g\beta \frac{\partial T}{\partial y}$	x, y, z	Cartesian Axis elements
g	The value of acceleration due to gravity (m/s ²)	ϵ	Turbulence dissipation rate
K	Turbulence kinetic energy	μ	Molecular Viscosity (N.s/m ²)
P	Pressure drop (Pa)	μ_t	Turbulent viscosity (N.s/m ²), $\mu_t = f_\mu \rho C_\mu \frac{K^2}{\epsilon}$
T	Temperature (°C)	ρ	Density (Kg/m ³)
		σ_ϵ	turbulent Prandtl number of ϵ



Acknowledgements

This work was supported by the (Better-Shelter.org) that supplied the tent samples used in this work.

Credit Authorship Contribution Statement

May Abdulazeez Rashid: Writing – review & editing, Writing – original draft, Validation, Software, Methodology. Issam M. Aljubury: Writing – review & editing.

Declaration of Competing Interest

The authors declare that they have no known competing financial interests or personal relationships that could have appeared to influence the work reported in this paper.

REFERENCES

Albadra, D., Vellei, M., Coley, D., and Hart, J., 2017. Thermal comfort in desert refugee camps: An interdisciplinary approach. *Building Environment*, 124, pp. 460–477.

Alhosainy, A.H.M., and Aljubury, I.M.A., 2019. Two stage evaporative cooling of residential building using geothermal energy. *Journal of Engineering*, 25(4), pp. 29-44.
<https://doi.org/10.31026/j.eng.2019.04.03>

Ali, I.M., and Albayati, H.D., 2017. Influence of covering materials and shading on the greenhouse cooling in Iraq. *Al-Nahrain Journal for Engineering Sciences*, 20(1), pp. 262-271.

Aljubury, I.M.A., and Ridha, H.D.A., 2017. Enhancement of evaporative cooling system in a greenhouse using geothermal energy. *Renewable energy*, 111, pp. 321-331.
<http://dx.doi.org/10.1016/j.renene.2017.03.080>.

Al-Juwayhel, F., El-Dessouky, H., Ettouney, H., and Al-Qattan, M., 2004. Experimental evaluation of one, two, and three stage evaporative cooling systems. *Heat Transfer Engineering*, 25(6), pp. 72-86.
<https://doi.org/10.1080/01457630490486292>.

Blocken B., and Persoon J., 2009. Pedestrian wind comfort around a large football stadium in an urban environment: CFD simulation, validation and application of the new Dutch wind nuisance standard. *Journal of Wind Engineering and Industrial Aerodynamics*, 97 (5-6), pp. 255-270.

Chung D.H. J., and Choo M.L.L., 2011. Computational fluid dynamics for urban design: the prospects for greater integration. *International Journal of Architectural Computing*, 9, pp. 33-54.

Crawford, C., Manfield, P., and McRobie, A., 2005. Assessing the thermal performance of an emergency shelter system. *Energy and Buildings*, 37(5), pp. 471-483.
<https://doi.org/10.1016/j.enbuild.2004.09.001>.

El-Dessouky, H., Ettouney, H., and Al-Zeefari, A., 2004. Performance analysis of two-stage evaporative coolers. *Chemical Engineering Journal*, 102(3), pp. 255-266.
<https://doi.org/10.1016/j.cej.2004.01.036>.

Erell E., Pearlmutter D., and Williamson T.J., 2012. *Urban microclimate: designing the spaces between buildings*, London, Earthscan.



- Faisal, I.J., Amir, A.A.H., Habib, I.S., and Hisham, T.A.E., 1997. Experimental investigation of the performance of two-stage evaporative coolers. *Heat Transfer Engineering*, 18(2), pp. 21-33. <https://doi.org/10.1080/01457639708939893>
- Fanger, P.O., 1970. Thermal comfort. Analysis and applications in environmental engineering. *Thermal comfort. Analysis and Applications in Environmental Engineering*, 1st ed, Copenhagen, Denmark, Danish Technical Press.
- Fanger, P.O., 1981. Prediction of local discomfort for man. In *Studies in Environmental Science*. (Vol. 10, pp. 221-227). Elsevier.
- Gooijer, H., Velan, M., Esen, I., Kamphuis, S., Groeneveld, R., Agrawal, P., and Brinks, G., 2019, June. Thermal comfort of textiles for tent application. In *AUTEX2019-19th World Textile Conference on Textiles at the Crossroads* (pp. 1-6).
- IDMC. 2017. International Displacement Monitoring Centre Database.
- IFRC, 28 June, 2012a- last update, IFRC/ICRC, emergency items catalogue-family tent specification [Homepage of IFRC],
- Jagadeesh, P., and K. Murali, K., 2005. Application of low-re turbulence models for flow simulations past underwater vehicle hull forms.
- Karyono, K., Abdullah, B.M., Cotgrave, A.J., and Bras, A., 2020. The adaptive thermal comfort review from the 1920s, the present, and the future. *Developments in the Built Environment*, 4, P. 100032. <https://doi.org/10.1016/j.dibe.2020.100032>.
- Kowalski, P., and Kwiecień, D., 2020. Evaluation of simple evaporative cooling systems in an industrial building in Poland. *Journal of Building Engineering*, 32, P. 101555. <https://doi.org/10.1016/j.jobe.2020.101555>.
- Matusiak, M., 2010. Thermal comfort index as a method of assessing the thermal comfort of textile materials. *Fibres & Textiles in Eastern Europe*, 18(2), pp. 45-50.
- Mays Ahyab Shoky, 2021, Experimental and numerical investigation on the thermal comfort of combined chilled, Master thesis submitted to the mechanical engineering department, University of Technology, Iraq.
- Mohamed, A., Khalil, E.E., and ElHarriri, G., 2020. Experimental investigation of a two-stage indirect/direct evaporative cooling system under different climatic conditions. In *AIAA Scitech 2020 Forum*, P. 1225. <https://doi.org/10.2514/6.2020-1225>.
- Mohammed, A.K., and Mohammed, A.K., 2013. Experimental performance of two-stage evaporating cooling system. *Scholars Journal of Engineering & Technology*, 1, pp. 122-127.
- Moran, F., Fosas, D., Coley, D., Natarajan, S., Orr, J., and Ahmad, O.B., 2021. Improving thermal comfort in refugee shelters in desert environments. *Energy for Sustainable Development*, 61, pp. 28-45. <https://doi.org/10.1016/j.esd.2020.12.008>.
- Musa, M.A., 2009. *Novel evaporative cooling systems for building applications*. Ph.D. dissertation, University of Nottingham.
- Poschl, R.A., 2017. *Modelling the thermal comfort performance of tents used in humanitarian relief*. Ph.D theses, Loughborough University.



Rupp, R.F., Vásquez, N.G. and Lamberts, R., 2015. A review of human thermal comfort in the built environment. *Energy and Buildings*, 105, pp.178-205.
<https://doi.org/10.1016/j.enbuild.2015.07.047>

Susanti, L., 2015, March. Thermal comfort evaluation of emergency tent using PMV and PPD model. In *Proceedings of the International MultiConference of Engineers and Computer Scientists* (Vol. 2, pp. 958-963).

Tan, A.Y.K., and Tan, C.K., 2021. Thermal comfort performances of temporary shelters using experimental and computational assessments. *Buildings*, 11(12), P. 655.
<https://doi.org/10.3390/buildings11120655>.

Tominaga Y., and Stathopoulos T., 2009. Numerical simulation of dispersion around an isolated cubic building: comparison of various types of k- ϵ models. *Journal of atmospheric environment*, 43(20), pp. 3200-3210.

UNHCR, 1999. Handbook for Emergencies. UNHCR, Geneva.

UNHCR, 2014. Statistical Yearbook 2014. www.un-hcr.org/statisticalyearbook/2014-annex-tables.zip. UNHRC. 2021. Refugee Data Finder. 2021.

Wang Y., 2017. *Experimental and numerical studies on improving the indoor thermal environment in a disaster-relief temporary prefabricated house located in the subtropics*, PhD thesis, The Hong Kong Polytechnic University.

World Bank Group, 2021. Open Knowledge Repository, Groundswell Part 2: Acting on Internal Climate Migration. <https://openknowledge.worldbank.org/handle/10986/36248>

Xatamovich, A.I., and Maidanovich, K.N., 2022. Climate change and its impact on increasing poverty. *International Journal of Multicultural and Multireligious Understanding*, 9(12), pp. 485-493.
<https://doi.org/10.18415/ijmmu.v9i12.4348>.

Zemitis, J., Borodinecs, A., Bogdanovics, R., and Geikins, A., 2021. A case study of thermal comfort in a temporary shelter. *Journal of Sustainable Architecture and Civil Engineering*, 29(2), pp. 139-149.
<https://doi.org/10.5755/j01.sace.29.2.29240>.

Zhang, L., Meng, X., Liu, F., Xu, L., and Long, E., 2017. Effect of retro-reflective materials on temperature environment in tents. *Case Studies in Thermal Engineering*, 9, pp.122-127.
<https://doi.org/10.1016/j.csite.2017.02.001>.

دراسة عددية لأداء نظام التبريد التبخيري باستخدام مياه الآبار المشغلة بالألواح الكهروضوئية على الراحة الحرارية لخيام الإغاثة

مي عبد العزيز رشيد^{*}، عصام محمد علي الجبوري

قسم هندسة الميكانيك، كلية الهندسة، جامعة بغداد، بغداد، العراق

الخلاصة

عندما يحتاج عدد كبير من الناس إلى الإجراء من منازلهم لأسباب مختلفة ، بما في ذلك الكوارث الطبيعية والصراعات المسلحة، فإن الوقت والمال أمران جوهريان. لذلك ، تعتبر خيام الإغاثة في حالات الطوارئ الخيار الأكثر فعالية لهذا الموقف. ومع ذلك، قد تكون البيئة الداخلية لهذه الأنواع من الخيام غير مريحة حرارياً ، خاصة في الأيام الحارة أو شديدة البرودة. تم استخدام تقنيات مختلفة للتغلب على هذه المشكلة بما في ذلك أنظمة التبريد التبخيرية. تهدف هذه الدراسة إلى استخدام نهج عددي لتقييم تأثير استخدام نظام التبريد التبخيري (غير المباشر / المباشر) ذو المرحلتين على تعزيز ظروف الراحة الحرارية الداخلية لخيمة الإغاثة. تم تنفيذ الجزء العددي باستخدام برنامج مكتوب بلغة فورتران لمحاكاة الحالة تحت معايير مختلفة ، بما في ذلك تغيير سمك وسادة السليلوز ومعدلات تدفق المياه الحجمية في المبادل الحراري الثاني لمرحلة التبريد غير المباشر. تم اختيار الشروط الحدية التي تم تطبيقها في التحليل العددي إلى البيانات التجريبية التي تم جمعها على مدار أيام محددة خلال صيف عام 2022، (تحديداً من 15 تموز إلى 15 أيلول). وفقاً للنتائج ، فإن وجود مبادلين حراريين في مرحلة التبريد غير المباشر لنظام التبريد يساعد في الحفاظ على نموذج الخيمة في درجة حرارة مريحة بسبب الأداء الاستثنائي لنظام التبريد المقترح في خفض درجات حرارة البصلة الجافة والرطوبة للهواء قبل الدخول في مرحلة التبريد التبخيري المباشر. بالإضافة إلى ذلك ، وجد أن انخفاض درجة الحرارة الداخلية زاد بحوالي 19 ٪ عند زيادة سمك وسادة السليلوز ورفع معدل تدفق المياه في المبادل الحراري الثاني لمرحلة التبريد غير المباشر.

الكلمات المفتاحية: خيمة الإغاثة والطوارئ القياسية، الراحة الحرارية، نظام التبريد التبخيري ذي المرحلتين، PMV.